Heliyon 10 (2024) e37914

Contents lists available at ScienceDirect

Heliyon

journal homepage: www.cell.com/heliyon

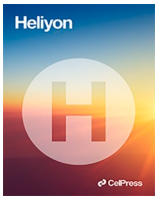

Research article

Blue light emitting graphene quantum dots/ Rhodamine B doped gold nanostars for ratiometric detection of methotrexate

Masoud Gazizadeh [a,b], Masoumeh Foroutan Koudehi [b,*], Hossein Fasihi [b], Jafar Soleymani [c], Ramin Zibaseresht [b,d,**]

[a] Toxicology Research Center, AJA University of Medical Sciences, Tehran, Iran
[b] Biomaterials and Medicinal Chemistry Research Center, AJA University of Medical Sciences, Tehran, Iran
[c] Pharmaceutical Analysis Research Center, Tabriz University of Medical Sciences, Iran
[d] Department of Chemistry and Physics, Faculty of Sciences, Maritime University of Imam Khomeini, Noshahr, Iran

ARTICLE INFO

Keywords:
Au nanostar
Dual-emission fluorescent sensor
Antifolate
Graphene quantum dots
Methotrexate
Quenching
Ratiometric fluorescence

ABSTRACT

In this work, an innovative ratiometric sensing platform was developed for the determination of methotrexate (MTX), an antifolate drug, a chemotherapy agent, and an immune system suppressant based on blue emission graphene quantum dots/Rhodamine B doped gold nanostars (B-GQDs/Au NSt-RB). The developed sensor was a dual-emission fluorescent probe with two major emission peaks at 440 nm (B-GQDs) and 580 nm (Au NSt-RB) by exciting at 330 nm. Based on the inhibiting effect of MTX on the system's fluorescence density, the stable ratiometric fluorescent probe was used for the rapid determination of MTX in aquatic solutions and spiked human serum samples. The results indicated good linear correlations over the logarithmic concentration range of 0.3 nM–50.0 μM. In addition, B-GQDs/Au NSt-RB can further realize highly sensitive detection of MTX with a low LOD value of 2.28×10^{-10} M. The RSD% values obtained for the intra-day and inter-day precision were 0.63–3.86 %. With recoveries of 98.2–100.1 % and 98.7–100.5 %, respectively. The short-term temperature and freeze-thaw tests confirmed the higher stability of the developed sensor. In addition, the calculated recoveries for MTX recognition in real samples were in the range of 98–102 %. These findings suggested the excellent potential of the ratiometric fluorescence B-GQDs/Au NSt-RB sensor for detecting MTX in real plasma samples.

1. Introduction

Methotrexate (MTX; Fig. 1), an antifolate drug, is a chemotherapy drug and immune system suppressant that was introduced as the first cancer therapy substance in 1940 [1]. MTX is widely used in the therapy of various cancers, autoimmune diseases, ectopic pregnancies, and for medical abortions [2]. It has been reported that MTX has an excellent therapeutic effect on almost 700 cancer cell lines [3]. MTX binds with higher affinity to dihydrofolate reductase (DR) and hinders the conversion of dihydrofolate to tetrahydrofolate by inhibiting the function of DR, disrupting DNA and RNA synthesis [4–6]. High MTX doses can cause kidney damage due to the crystallization of MTX and its metabolites in the nephrons, which can lead to severe toxicities [7]. Therefore, monitoring the blood level of MTX can be one of the most important clinical challenges.

* Corresponding author.
** Corresponding author. Biomaterials and Medicinal Chemistry Research Center, AJA University of Medical Sciences, Tehran, Iran.
E-mail addresses: masoumeh.foroutan@yahoo.com (M. Foroutan Koudehi), rzi12@uclive.ac.nz (R. Zibaseresht).

https://doi.org/10.1016/j.heliyon.2024.e37914
Received 20 August 2023; Received in revised form 11 September 2024; Accepted 12 September 2024
Available online 13 September 2024

Antibody-based methods are the most commonly used techniques for estimating blood concentrations of MTX in clinics [5]. However, various other analytical approaches for MTX detection have been published in the literature, including high-performance liquid chromatography-ultraviolent (HPLC-UV) detector [8], liquid chromatography-mass spectrometry (LC−MS) [9], capillary electrophoresis (CE) [10], LC/MS/MS [11], and surface-enhanced Raman scattering (SERS) technique [12]. These analytical methods have some drawbacks that limit their widespread applications, such as high cost, complicated operation, extensive preprocessing, and an unsatisfactory detection limit. Therefore, developing simple, sensitive, and low-cost techniques for estimating the blood level of MTX has received considerable attention among researchers.

In recent years, fluorimetric methods, which are based on various substances with fluorescence properties, have appealed attentions of researchers for the detection of different analytes. However, among various fluorescence sensing techniques, ratiometric fluorescent sensors show a considerable advantage [13,14]. A ratiometric measurement, involving the simultaneous recording of fluorescence levels at two wavelengths using one excitation wavelength and calculating their ratio, provides greater precision than other fluorimetric methods [15]. In general, ratiometric fluorescence approaches are renowned for their selectivity, ease of use, fast experimental protocols, minimal sample requirement, high sensitivity within nano or lower concentration ranges, cost-effectiveness, and superior reproducibility compared to other methods. They find wide applications in environmental analysis, facilitating the identification and removal of industrial effluents, as well as in biology for metabolite, enzyme, and cancer cell identification amidst healthy cells. One of the primary objectives of ratiometric methods is to minimize matrix disturbances [16].

According to previous reports, different ratiometric fluorescence approaches based on semiconductor quantum dots have been developed. Because of their sharp and continuous excitation spectra and size-tunable fluorescence, these materials are preferable for producing multicolored fluorescent systems [17]. Carbon-based dots like graphene quantum dots (GQDs) showed unique properties in the fabrication of sensing probes, including high absorbance coefficient, chemical and physical stability, and favorable biocompatibility [18–20]. Considering the beneficial features of GQDs, in this work, a novel dual-emissive ratiometric probe was constructed by blue emission GQDs (B-GQDs) coupled with rhodamine B doped gold nanostars (Au NSt-RB) (B-GQDs/Au NSt-RB). The prepared dual ratiometric probe was applied for estimating MTX in aquatic solutions and real samples (Scheme 1). The different experimental parameters were optimized. The detection result showed a good linear relationship between log (B-GQDs/Au NSt-RB) and MTX concentration with high selectivity. So, we report a novel, versatile, sensitive, and specific approach, capable of sensing MTX.

2. Materials and methods

2.1. Materials

Propanol, acetone, AOT (Aerosol-OT or sodium bis(2-ethylhexyl)), methanol, acetonitrile, ethanol, cetyltrimethylammonium bromide (CTAB), Triton X-100, Brij, and tris (hydroxymethyl) aminomethane (TRIS), tween 20, chloroform, (Rhodamine B) RB, sodium acetate, sodium phosphate salts ($Na_2HPO_4.7H_2O$ and $NaH_2PO_4.H_2O$), acetic acid, and sodium dodecyl sulfate (SDS) were prepared from Merck company (Germany). MTX was provided from Dana Pharmaceutical Company (Tabriz, Iran). The buffer solutions' pH levels were adjusted employing HCl and NaOH.

2.2. Synthesis

2.2.1. Synthesis of blue emitting GQDs (B-GQDs)

GQDs were synthesized by dissolving 1.0 g of graphene oxide in H_2SO_4 and mixing well for 2 h to suspend entirely. Then, 40 wt% of $KMnO_4$ powder was added to the prepared solution. The prepared reaction solution was heated for 1 h at 45 °C after being stirred for 2 h. In the next step, better effervescence was produced by adding 40 mL of deionized water and then the mixture's temperature reached 80 °C. Subsequently, H_2O_2 was dropped into the solution to ensure complete $KMnO_4$ consumption. After pouring the solution over ice and inhibiting the reaction, the prepared solution was ultrasonicated for 5 min. The solution was cooled, followed by adjusting the pH to around 8 using a 10 % NaOH solution, which resulted in the production of flocculent black deposits. Using 1.0 M HCl dropwise, the pH of the mixture was adjusted to 4, yielding a deep yellow-colored solution. Finally, B-GQDs were obtained after the filtration of the prepared solution, removing the large particles of graphene and the dialysis of the supernatant through a three kDa membrane [21].

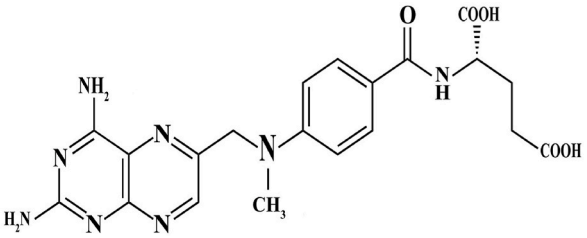

Fig. 1. Chemical structure of the MTX.

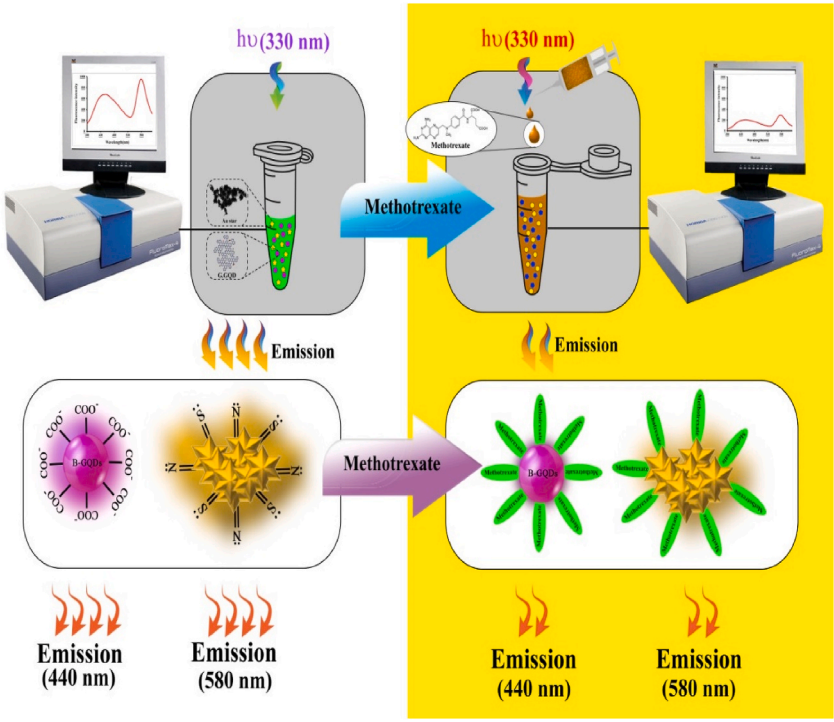

Scheme 1. Schematic illustration for detecting MTX based on fluorescence quenching of the dual ratiometric fluorescent probe B-GQDs/Au NSt-RB.

2.2.2. *Synthesis of Au NSt*

Gold nanostars (Au NSt) were synthesized using a seed-mediated growth procedure. In this case, 25 μL of sodium citrate (5.0 mM) was mixed with a solution containing 10 mL of $HAuCl_4$ (50 mM) and 10 mL of $Na_3C_6H_5O_7$ solution (250 mM). After 10 min of stirring, 0.4 mL of the produced sodium borohydride ($NaBH_4$, 40 mM) solution was quickly added and agitated for another 5 min. The prepared Au nanoparticles (orange-red solution) were utilized to prepare the Au NSt. Then, 20 mL of cetyltrimethylammonium bromide (CTAB) solution (50 mM) was added at 30 °C. Next, 60 μL of $AgNO_3$ solution (16.3 mM) was added to the reaction solution. After 60 s, the $HAuCl_4$ solution was added and mixed for another 60 s. The solution was colorless after 100 μL of L-ascorbic acid (80 mM) was supplemented. After adding 50 μL of Ag seeds and 1 h of stirring, the final brownish product was isolated. The solution was then heated up to 30 °C to dissolve the CTAB residues. Finally, the produced nanoparticles were separated by various centrifugation steps [22].

2.2.3. *Synthesis of RB-capped Au NSt*

The previously synthesized Au NSt was extracted from the reactive solution mixture through centrifugation at 6000 rpm for 15 min and employed for the synthesis of RB-capped Au NSt (Au NSt-RB). Then, the prepared Au NSt was re-suspended in distilled water and mixed with a desired amount of RhB (0.2 μM), and incubated overnight.

2.3. *Instrumentation*

The Fourier transform infrared (FT-IR) spectra of nanoparticles were recorded using a TENSOR27 spectrometer (Bruker, Germany) in the 400–4000 cm^{-1} range. Transmission electron microscope (TEM) was employed to test the morphology of the produced particles (FEI Talos F200X, USA). The fluorescence studies were performed on a fluorescence spectrometer (Jasco FP-750, Kyoto, Japan) by exciting the samples at 330 nm ($\lambda_{ex} = 330$ nm) and measuring the maximum emission intensities (λ_{ex}) of B-DQDs and Au NSt/RhB at 440 nm and 580 nm, respectively. In addition, using an AFM (a nanosurf mobile S, Grammetstrasse, Switzerland). This study used to investigate the surface topography of the prepared materials spectrophotometer (T60, PG Instruments LTD, UK), the absorption spectra of the samples were recorded.

2.4. *Fluorometric determination of MTX in aqueous solution by B-GQDs and AuNSt/RB*

In a typical experiment, MTX with a series of concentrations (0.7 nM-10.0 μM) and constant concentrations of Au NSt/RB (600 mg/L) and B-GQDs (100 mg/L) was mixed in a phosphate buffer solution (100 mM, pH = 8.5). The emission spectra of the mixtures were recorded in the wavelength range from 300 to 650 nm (under 330 nm excitation) and were used for the evaluation of the concentration of MTX in plasma samples.

2.5. Selectivity of B-GQDs and Au NSt/RB

To investigate the detection selectivity of the ratiometric probe, a reaction solution containing B-GQDs (100 mg/L) and Au NSt/RB (600 mg/L) was treated with 70 μM of different interference species, such as different cations and anions (Na^{+}, Cl^{-}, Cu^{2+}, Mg^{2+}, Pb^{2+}, K^{+}, Ca^{2+}, and Zn^{2+}), and vitamins (D_3, E, C and B_1, B_2). The final volume of the prepared solutions was 4.5 mL. The samples' emission intensities were then measured at 440 and 580 nm.

2.6. Measurement of fluorescence quantum yields (QY)

In this study, the QY of the B-GQDs was measured using tryptophan as a standard with a QY value of 13 %. The following equation was used to calculate absolute values (Eq. (1)) [23,24].

$$QY_{S-CDs} = QY_{TrP}\left(\frac{A_{Trp}}{A_{S-CDs}}\right)\left(\frac{F_{S-CDs}}{F_{Trp}}\right)\left(\frac{\eta_{S-CDs}}{\eta_{Trp}}\right)^{2} \quad (1)$$

Where, A denotes the absorbance density, and η is the refractive index value of the solvent (in aqueous media it equals 1). In this work, the QY of B-GQDs was calculated using tyrosine as a reference substance with a QY of 16 % [25].

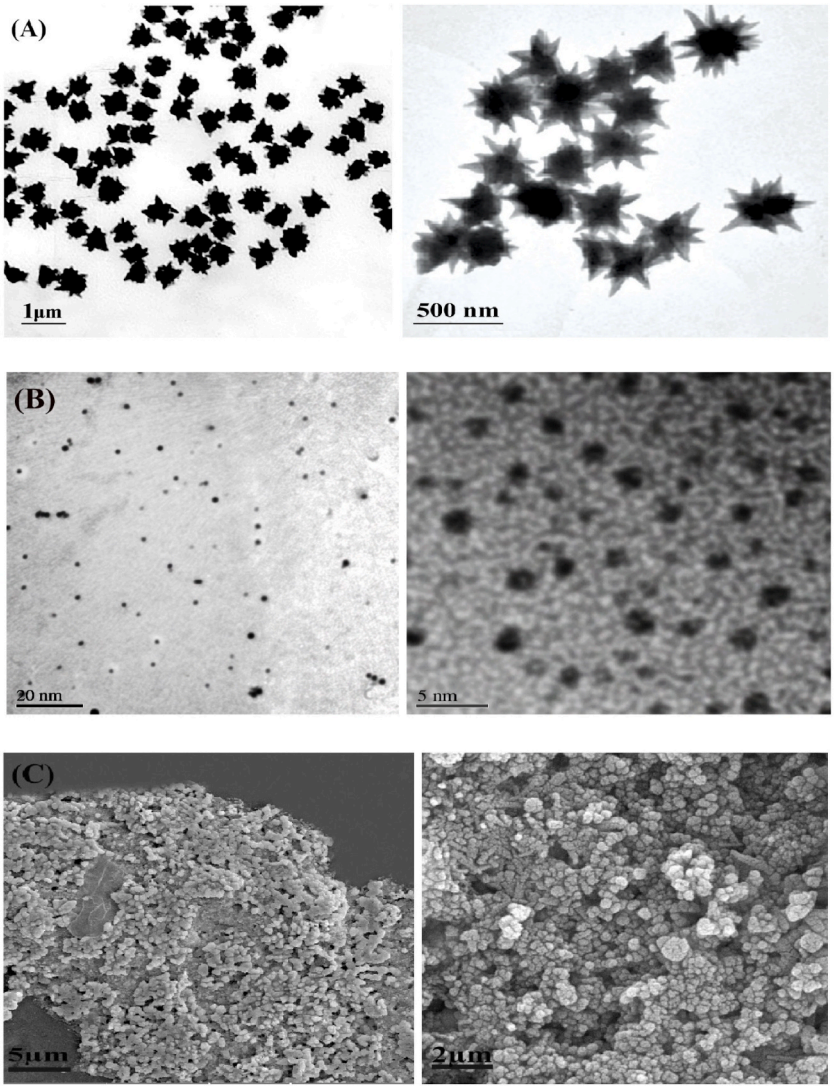

Fig. 2. TEM images of Au NSt (A), B-GQDs (B), and SEM images of B-GQDs/Au NSt in the presence of MTX (C).

2.7. Fluorometric analysis of MTX in real samples

To quantify MTX in the real matrix, healthy adult plasma samples were obtained from the Iranian Blood Transfusion Organization (IBTO, Tabriz, Iran). The prepared normal samples were deproteinized and spiked with known concentrations of MTX (0.005, 0.01, 0.05, 0.1, 0.5 and 5 μM). Finally, the standard curve was utilized to estimate the MTX concentration in real samples. Written consent was obtained from all participants, and the questionnaire and methodology for this study were approved by the Human Research Ethics Committee of AJA University of Medical Sciences (IR.AJAUMS.REC.1401.213). It is confirmed that this study complies with all regulations.

2.8. Detection of MTX in real samples

To assess the feasibility and applicability of the constructed B-GQDs/Au NSt fluorescent platform for estimating MTX, healthy human plasma samples were spiked with MTX concentrations. To perform spike operation on real samples, in short, 0.5 ml of MTX standard solution was added to 1 ml of healthy human plasma, and after a few minutes, 1 ml of 1M trichloroacetic acid solution was added to it sediment the proteins. After separating the sedimented proteins by centrifugation, the MTX and the spiked plasma, a clear liquid above the sediments, were taken out and used to perform tests.

The amount of MTX in samples was obtained employing the standard method and the added-found approach. Table 5 represents the determination of MTX concentrations in spiked samples. It can be that the calculated recoveries of the six different concentrations were in the 98.0–102.4 % range. These findings suggested the excellent potential of the ratiometric fluorescence B-GQDs/Au NSt-RB sensor for detecting MTX in natural plasma samples.

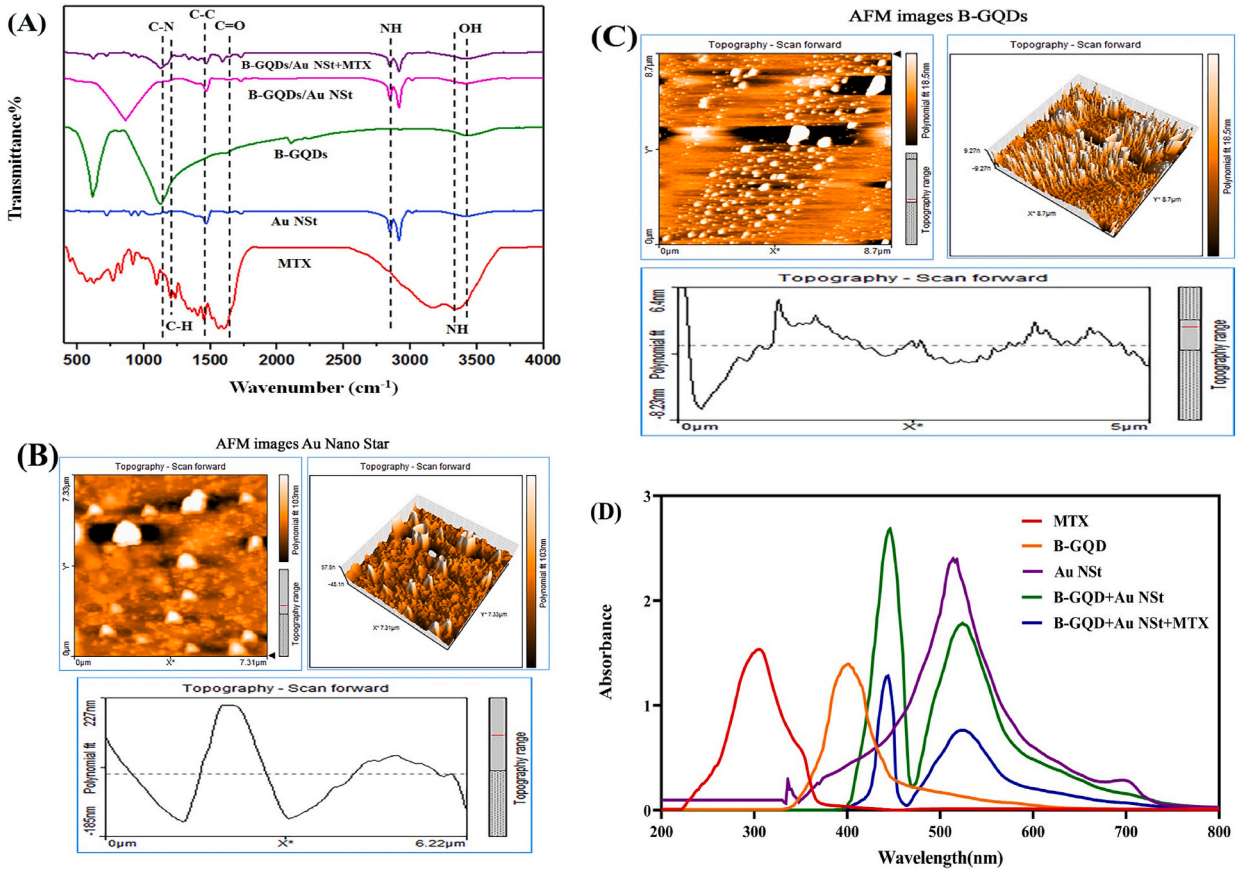

Fig. 3. FTIR spectrum of Au NSt, B-GQDs, MTX, and B-GQDs/Au NSt in the presence of MTX (A), Atomic force microscopy (AFM) topographic of Au NSt (B), B-GQDs (C), and UV–Vis absorption spectra of Au NSt-RB, B-GQDs, MTX, B-GQDs/Au NSt, and B-GQDs/Au NSt in the existence of MTX (D).

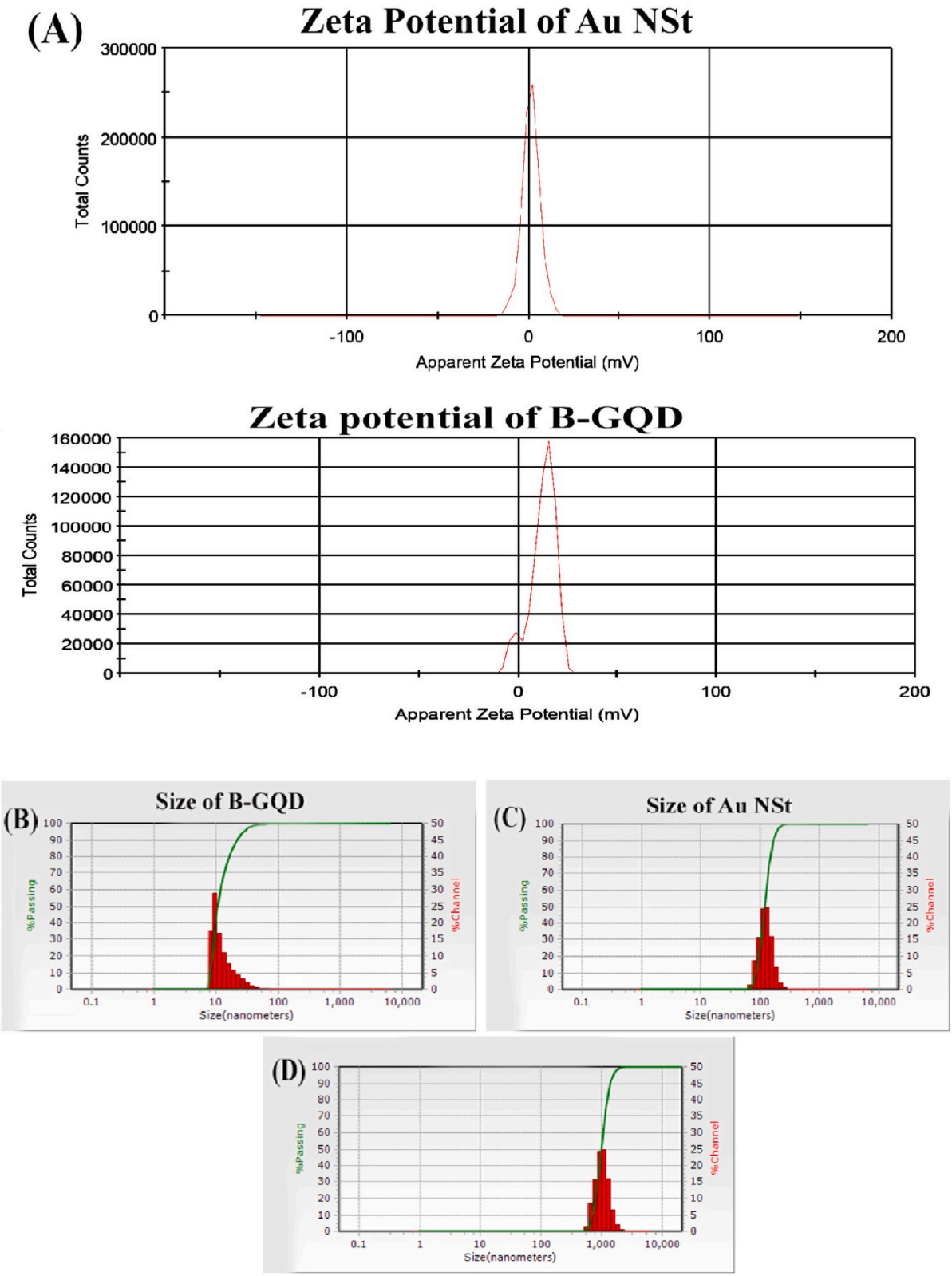

Fig. 4. Zeta potential of Au NSt and B-GQDs (A), DLS characterization of B-GQDs (B), Au NSt (C), and B-GQDs/Au NSt in the existence of MTX (D).

3. Results and discussion

3.1. Characterization

Morphology analysis of the prepared B-GQDs and Au NSt was carried out using TEM analysis (Fig. 2A and B). As confirmed by TEM images, the prepared B-GQDs and Au NSt showed remarkable monodispersity in shape. Also, the average sizes of B-GQDs and Au NSt were 10 nm and 150 nm, respectively. In addition, the morphology of the prepared B-GQDs and Au NSt in the existence of MTX are exhibited Fig. 2C. It is obvious that B-GQDs and Au NSt were aggregated after adding MTX to the solution.

Furthermore, Fig. 3A shows the FTIR spectra of the synthesized particles. This figure confirmed the successful synthesis of Au NSt and B-GQDs. In addition, the FTIR spectra of B-GQDs/Au NSt/MTX were a mixed form of the spectra of Au NSt, B-GQDs, and MTX. The sharp bands concerning the stretching vibrations (N–H) of primary and secondary amines, and aldehydic C-H stretching were observed at around 2852 cm^{-1} and 3454 cm^{-1}, respectively, which also related to the vibrations of the -OH functional groups [26]. The characteristic vibrations of the C=O and C-N stretching bands appeared at around 1600 cm^{-1} and 1149 cm^{-1} [27]. The observed spectral changes and shifts and the alterations in the band intensities in the FTIR spectra confirmed the binding of B-GQDs and Au NSt and the interaction of MTX with B-GQDs/Au NSt.

In the FT-IR spectrum of free MTX, a band at 3407 cm^{-1} indicates the existence of an NH group. Additionally, the indicated peaks in the region of 1675–1500 cm^{-1} are concerning C=C vibration in the aromatic ring and R-NH_2 vibrations. Peaks at 1460 cm^{-1} and 1209 cm^{-1} correspond to the stretching vibration of the C-C or C-H bonds, respectively. The FT-IR spectrum of B-GQDs/Au NSt + MTX showns similar bonds to that of free MTX, showing that MTX has been successfully uploaded into the B-GQDs/Au NSt. This is due to the interaction between B-GQDs/Au NSt and MTX.

Fig. 3(B and C) depicts the surface morphologies of the prepared The particle size of Au NSt and B-GQDs was similar to the findings from the DLS analysis. DLS and ZP are commonly used to rapidly measure the hydrodynamic size and surface charge of synthesized nanomaterials in suspension, respectively [28].

ZP can be either positive or negative, and its value can be related to the storage stability of particles. It has been reported that the ideal value of ZP is −30 to +30 mV [29]. According to the results, the obtained ZP values for Au NSt and B-GQDs were 1.35 and 13.8 mV Fig. 4A. However, the ZP amount of B-GQDs/Au NSt in the existence of MTX was increased. These results indicated the attachment of MTX to B-GQDs/Au NSt.

(Fig. 4B and C) shows the size distribution analysis of Au NSt, B-GQDs, as well as B-GQDs/Au NSt/MTX by DLS. The results of the particle size analysis of the prepared materials showed a significant increase in the particle size of the B-GQDs/Au NSt upon the addition of MTX, confirming the attachment of MTX to the B-GQDs/Au NSt Fig. 4D.

3.2. Spectroscopic analysis

The absorption spectra of the B-GQDs, MTX, Au NSt-RB, and B-GQDs/Au NSt (in the existence and absence of MTX) were recorded in the range of 300–800 (Fig. 3D). A suspension of B-GQDs has a characteristic absorption peak at 400 nm, attributed to the $n\rightarrow\pi^*$ electron transition of the C=O groups on the aromatic rings [8,30]. MTX and Au NSt exhibit a spectrum with a sharp maximum absorption at 310 and 514 nm, respectively. In addition, the UV–vis absorption spectrum of B-GQDs/Au NSt-RB exhibit two distinct bands at 444 nm and 524 nm, which were associated with B-GQDs and Au NSt-RB, respectively. However, after mixing two fluorophores a clear red shift by 44 nm and 10 nm was observed in the absorption spectra of B-GQDs and Au NSt-RB, respectively. This red shift demonstrated that the addition of B-GQDs to Au NSt-RB solution can affect the absorption properties of both nanoprobes.

Moreover, the alteration in the UV–vis spectra of GQDs/Au NSt-RB following the addition of MTX (1.0 μM) was assessed, and a hindering effect of MTX on the absorption spectra of B-GQDs/Au NSt-RB was observed. The overlap between the UV–vis absorption of B-GQDs/Au NSt-RB and MTX was insignificant.

3.3. Resonance light scattering (RLS)

RLS results revealed that B-GQDs have diameters between 6.0 and 10.0 nm. Therefore, the solution of these quantum dots can exhibit considerable dispersion, and the larger particles have higher scattering values. In this work, the potential for aggregation and accumulation of the particles in the existence of various concentrations of MTX (0.001, 0.07, 0.1, 0.5, 1, and 10 μM) into the reaction solution containing quantum dots were recorded. Based on the outcomes, as the concentration of MTX increased, so did the solution's dispersion (Fig. 1SA). These findings demonstrated that MTX molecules can bind to the surface of GQDs and induce the particles to cluster together, causing the quantum dots' size to change. Therefore, these outcomes confirmed the aggregation of B-GQDs/Au NSt-RB in the existence of MTX.

3.4. Optimization of experimental parameters

Our studies revealed that Au NSt does not have any characteristic emission peak. At same time the used RB to create fluorescence properties of Au NSt according to and following the available sources for this work. Several parameters, including pH, the type and concentration of buffer, temperature, solvent, and surfactant, incubation time, and the ratio of fluorophores were investigated by calculating the fluorescence ratio changes (F_{580}/F_{440}) in the presence of 1.0 μM MTX to improve the performance of the prepared ratiometric biosensor. Firstly, we optimized the type and concentration of the buffer. In this regard, various types of buffer solutions

(Tris-HCl, phosphate, and acetate buffer) with different concentrations (10–200 mM) and pH levels (from 2.5 to 11.5) were prepared, and then the fluorescence ratio of the sensor was recorded (Fig. 1SB to D). represents that the maximum fluorescence quenching was obtained using a 100 mM phosphate buffer solution with pH = 8.5. Thus, these values were selected as optimal. It has been reported that due to the protonation or deprotonation reaction of the fluorophore, the pH of the environment around the fluorescence probe usually has some effect on its performance.

Furthermore, the fluorescence ratio of the sensor decreased gradually with the time until time reached 10 min and then increased (Fig. 2SA). So, in the present work, the emission intensities of the samples were measured after 10 min of incubation.

In addition, the quenched emission intensity of the ratiometric sensor was evaluated at different temperatures (0–45 °C). Fig. 2SB depicts the obtained results. It is obvious that the system's response was unaffected by the temperature, and no considerable alterations were observed in the emission ratio of the prepared nanosensor. These outcomes suggested the stability of the prepared ratiometric sensor at various temperatures. Therefore, 25 °C was chosen as the optimal temperature.

In the next step, the dual ratiometric sensor's signal was studied by adjusting the probe ratios to identify the best ratios of B-GQDs to Au NSt-RB. The obtained results showed that the system experienced the most significant fluorescence hindering when the ratio of B-GQDs to Au NSt-RB was 1:6 (100 mg/L B-GQDs and 600 mg/L Au NSt-RB) without and with MTX (Fig. 2SC).

The solvent type and volume were optimized as well. For this purpose, under optimum conditions, the possible effects of solvents of various types (such as water, methanol, ethanol, propanol, acetone, chloroform, and acetone) and concentrations (50–2000 μL) on the emission quenching of the sensor were tested (Fig. 3SA and B). indicate the obtained results. The highest fluorescence quenching was obtained in 500 μL of chloroform with and without MTX. Therefore, we chose chloroform as the optimal reaction solvent for amplification.

To achieve the optimized analytical performance of the ratiometric fluorescent probe B-GQDs/Au NSt-RB, the impact of various surfactants, such AOT, CTAB, X100, SDS, tween 20, and Brij, on the system's signal was assessed (Fig. 3SC and D). shows that at the

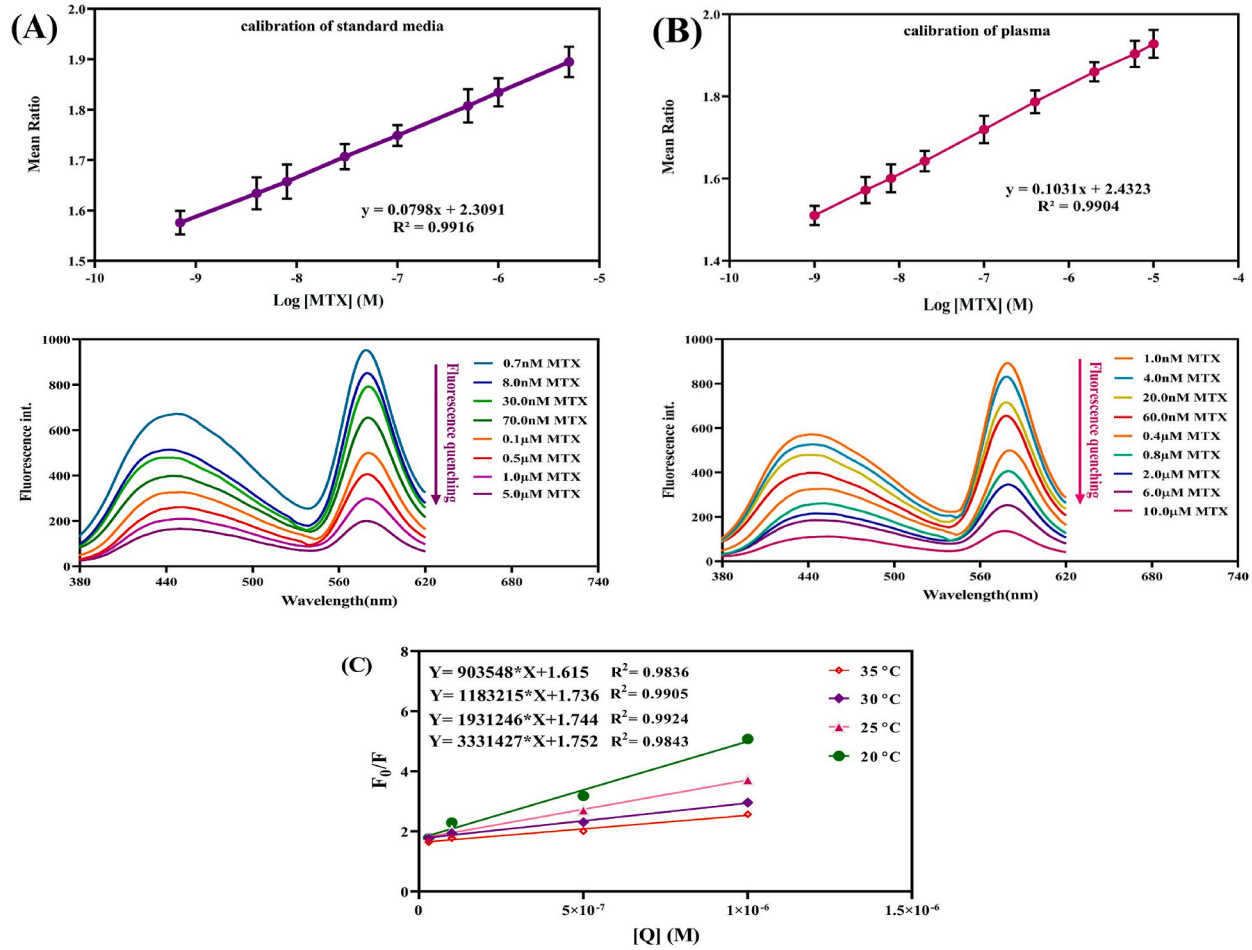

Fig. 5. The effect of MTX on the fluorescence intensity of B-GQDs/RB-Au NSt and the linear relationship between the fluorescence quenching ratio of B-GQDs/RB-Au NSt and the logarithm of MTX concentration in PBS buffer solution (0.01 M), pH = 8.5 and 25 °C (A), and the response of B-GQDs/RB-Au NSt towards MTX detection in human plasma samples in PBS buffer solution (0.01 M), pH = 8.5 and 25 °C (B) and mechanism of quenching (C).

critical micellar concentrations (CMC) and below, the highest response of the dual ratiometric probe was achieved in the presence of Brij as a surfactant with and without MTX.

The influence of ionic strength and UV light was examined on the dual ratiometric fluorescent probe. According to the data presented in Fig. 4SA and B, the emission intensity of the system was slightly reduced when the ionic strength was raised to 20 mM, with the maximum quenching of fluorescence observed at 20 mM NaCl concentration. Therefore, subsequent experiments were conducted with a 20 mM NaCl concentration. Additionally, the stability of our newly developed sensor was inspected. For this purpose, the fluorescence of the probe was investigated after exposure to UV light irradiation, revealing slight alterations in the nanoprobe's response even after 360 min of continuous irradiation. The results indicated that the B-GQDs/Au NSt-RB sensor was resistant to photobleaching and maintained performance over an extended period of analysis and testing [31].

3.5. Analytical figures of merit

Due to the importance of MTX and its widespread usage by cancer patients, it is highly necessary to detect the concentration of this medication. Herein, using a fluorescence sensor with dual-emission peaks of B-GQDs/Au NSt-RB, the concentration of MTX in aquatic solution was estimated. In this regard, under optimum conditions, different amounts of MTX (0.7 nM–10.0 μM) were added to the reaction solution, and then the emission of the system was recorded in the 300 nm–600 nm range. The results showed that the fluorescence emission peaks of the B-GQDs/Au NSt-RB decreased significantly by increasing the concentration of MTX, and the emission peak almost completely disappeared when the MTX concentration reached 10.0 μM, confirming the high sensitivity of the system towards MTX. Subsequently, the plot of the calibration curve was conducted using the logarithmic concentration of MTX versus quenched fluorescence of the system (Fig. 5A). According to this figure, there was a strong linear relationship in the range of 0.7 nM–10.0 μM with the equation of $y = 0.0798x+2.3091$. The detection limit (LOD) of the probe was calculated as signal-to-noise ratio (equals = 3) to be 2.28×10^{-10} M. The measurement of MTX levels was conducted under optimal conditions in normal plasma samples using the given procedure to assess the applicability of the proposed sensor. According to the observed data, the fluorescence intensity decreased as the MTX concentration increased, which was proportional to the MTX concentration. In addition, a linear relationship was exhibited between the emission ratio (F_{580}/F_{440}) and the concentration of MTX in the 1.0 nM to 10.0 μM with a correlation of $R^2 = 0.9904$ (Fig. 5B). On the other hand, we compared our developed dual ratiometric sensor response with previous studies (Table 1). As the data showed a lower LOD value for the proposed sensor for the detection of MTX than other methods. So, it can be stated that our method is preferable to other methods in terms of sensitivity.

3.6. Determining the quenching mechanism

According to the literature, fluorescence hindering of a probe in the presence of a ligand can occur through different mechanisms, including static and dynamic quenching, inner filter effect (IFE), photoinduced electron transfer (PET), surface energy transfer (SET), Förster resonance energy transfer (FRET), and Dexter energy transfer (DET) [38–40]. However, due to the lack of obvious overlap between the emission spectrum of B-GQDs/Au NSt-RB and the absorption spectrum of MTX, fluorescence quenching cannot occur via FRET, IFE, or PET. In other words, at the obtained optimum pH value (pH = 8.5), the amine functional groups of MTX have a neutral charge, which is due to the pK_a amount of MTX (between 4.5 and 5.8). In addition, because of the positive ZP of B-GQDs/Au NSt-RB, there is no strong electrostatic attraction between MTX and B-GQDs/Au NSt-RB. Therefore, MTX cannot bind to the surface of the B-GQDs/Au NSt-RB. Based on these rationales, the FRET mechanism is dismissed, and the system lacks a FRET acceptor-donor arrangement [41,42]. However, appeared new peaks confirmed the creation of the new complex system is probable. Therefore, the emission strength of the developed ratiometric system can be quenched through a static quenching mechanism due to a ground-state complex formation between B-GQDs/Au NSt-RB and MTX.

Stern-Volmer equation (Eq. (2)) was used to discuss the interaction mechanism between methotrexate (MTX) and B-GQDs/Au NSt-RB (Fig. 5C) [41]. Our results revealed a static quenching mechanism in which the stability of the ground state complex decreases by temperature rises, resulting in a decrease in the Stern-Volmer constant (K_{SV}).

$$\frac{F_0}{F} = 1 + K_{sv}[Q] \tag{2}$$

F represents the fluorescence strength of B-GQDs/Au NSt-RB with MTX, and F_0 represents the fluorescence strength of B-GQDs/Au NSt-RB without MTX. K_{SV} represent the Stern-Volmer constant and [Q] the amounts of MTX, respectively. Notably, the K_{SV} amounts

Table 1
A comparison of some previously described approaches for MTX detection with the proposed system.

Method	Linear range (μg/mL)	LOD (μg/mL)	Ref.
Surface-enhanced Raman spectroscopy (SERS)	4.5×10^{-4}-9.0×10^{-2}	4.5×10^{-4}	[32]
Capillary electrophoresis	1.0–6.0	3.5×10^{-1}	[33]
HPLC	1.1×10^{-2}-2.2	1.0×10^{-3}	[34]
RP HPLC	1.0×10^{-2}-10.0	1.8×10^{-1}	[35]
Electrochemical method	2.0×10^{-3}-3.2	1.3×10^{-3}	[36]
Fluorescence	1.6×10^{-3}-2.4	9.0×10^{-4}	[37]
B-GQDs/Au NSt-RB	**1.3×10^{-4}-22.7**	**4.5×10^{-5}**	**This work**

decrease with raising temperature, indicating the prevalence of static quenching as the predominant fluorescence quenching mechanism.

The binding parameters and the number of binding sites on nanoprobes for MTX can be determined by using Eq. (3) [41]:

$$log\frac{(F_0 - F)}{F} = log\, K_b + nlog[Q] \quad (3)$$

where n represents the number of binding sites and K_b the binding constant, respectively, which can be determined by plotting log [(F_0 - F)/F] vs. log [Q]. The estimated value of the binding constant (K_b) is $1.23 \times 10^{-4}\ M^{-1}$, providing evidence for the existence of binding sites in both MTX and B-GQDs/Au NSt-RB. Moreover, the results confirmed that n is equal to 1, indicating the existence of a unique binding site for MTX molecules on B-GQDs/Au NSt-RB.

3.7. Recovery and accuracy

For studying the precision of the developed system, inter-day and intra-day were calculated and stated as relative standard deviations (RSD%). These results were obtained from four replicate determinations of the MTX reference standard solution during a day (intra-day precision) and three consecutive days (inter-day precision). As exhibited in Table 2, the obtained RSD% amounts were 0.63 and 3.86 % for the intra-day and inter-day precision, respectively. The analytical recoveries were calculated from treated plasma samples in the range of 98.2–100.1 % and 98.7–100.5 %, respectively. These results confirmed that the probe has high accuracy and precision in the detection of MTX in plasma samples.

3.8. Stability study

The proposed approach was tested in plasma for short-term stability at 25 °C and 4 °C, as well as three freeze-thaw cycles at −20 °C. Short-term studies were conducted at five-time points. Samples were stored at room temperature and 2–8 °C for the duration of the studies and studied at each time point [21]. By comparing the obtained results to those from freshly manufactured samples, the stability of the developed sensor was evaluated. As shown in Table 3, the calculated recoveries for short-term temperature and freeze-thaw treatment were 98.3–100.0 % and 97.6–105.0 %, respectively. These results confirmed the higher stability of the developed sensor in actual samples.

3.9. Interference studies

To study the specificity of the probe, the interferences of commonly available interfering agents in biological samples were examined under optimum conditions with 70 nM of MTX. Interference studies of some cations and anions, including amino acids, vitamins, and pharmaceutical formulations, were performed until a variation more significant than 5 % in the emission intensity of the system was achieved [42–44]. Fortunately, none of the ions produced a noticeable fluorescence response (Table 4). Therefore, the developed probe is not affected by other interferences compared to the Named table, suggesting the high specificity of the developed probe for detecting MTX.

4. Conclusion

Briefly, a new sensitive and selective dual ratiometric fluorescent B-GQDs/Au NSt-RB probe was developed for the rapid estimation of MTX. After characterization studies of the prepared systems, the fluorescent probe was utilized for estimating MTX concentration based on its hindering effects on the emission intensity of the fluorescent B-GQDs/Au NSt-RB nanoprobe. The prepared sensor had two prominent characteristic emission peaks at 440 nm (corresponding to B-GQDs) and 580 nm (corresponding to Au NSt-RB). Various experimental factors affecting the response of the sensor were optimized. The emission intensity of the system was evaluated in the attendance of different amounts of MTX, and the results indicated that the fluorescence intensity of the system gradually decreased with increasing the concentration of MTX. In addition, the LOD amount was calculated to be 0.13 nM. Moreover, all stability and recovery tests of the proposed method for the determining of methotrexate showed acceptable and positive results. These findings

Table 2
Detailed information for the determination of MTX in human plasma samples.

Sample	Concentration (M)	Precision (RSD%)	Accuracy Recovery (%)
Intra-day	4.0×10^{-9}	0.63	100.1
	6.0×10^{-8}	2.55	101.0
	4.0×10^{-6}	3.86	102.3
	2.0×10^{-5}	0.83	98.2
Inter-day	5.0×10^{-9}	0.63	99.8
	1.0×10^{-8}	2.25	100.5
	5.0×10^{-6}	3.86	99.2
	1.0×10^{-5}	1.32	98.7

Table 3
Short-term temperature and freeze-thaw stability of the proposed approach in the plasma sample.

Sample	Con. (M)	Short-time temperature (Detected)	Recovery (%)	Freeze-thaw (Detected)	Recovery (%)
Plasma	8.0×10^{-9}	7.9×10^{-9}	98.7	8.2×10^{-9}	102.5
	2.0×10^{-8}	1.7×10^{-8}	85.0	1.5×10^{-8}	96.4
	2.0×10^{-6}	2.2×10^{-6}	110.1	1.7×10^{-6}	97.6
	6.0×10^{-6}	6.3×10^{-6}	105.0	5.8×10^{-6}	98.1

Table 4
The impact of certain common interfering species on MTX detection (70 nM).

Interfering agent	Concentration of interfering agent (M)	Ratio	RSD%
Na^{+}	6.3×10^{-5}	900	−0.8
K^{+}	6.3×10^{-5}	900	−0.8
Mg^{2+}	6.3×10^{-5}	900	−0.8
Zn^{2+}	7.0×10^{-5}	1000	3.9
Ca^{2+}	7.0×10^{-5}	1000	10.5
Cl^{-}	7.0×10^{-5}	1000	10.5
Cu^{2+}	3.5×10^{-6}	50	−8.9
Pb^{2+}	3.5×10^{-5}	500	−5.3
Starch	7.0×10^{-5}	1000	3.2
Lactose	7.0×10^{-5}	1000	3.2
Uric Acid	3.5×10^{-5}	500	−10.6
Sucrose	7.0×10^{-5}	1000	0.0
Vitamin B1	4.2×10^{-5}	600	−5.8
Vitamin B2	7.0×10^{-6}	100	−11.1
Vitamin D3	6.3×10^{-5}	900	3.9
Vitamin E	6.3×10^{-5}	900	3.9
Vitamin C	7.0×10^{-5}	1000	3.9
Naproxen	4.9×10^{-5}	700	−7.1
Mesalazine	6.3×10^{-5}	900	−0.8
Amlodipine	6.3×10^{-5}	900	−0.8
Cephalexin	6.3×10^{-5}	900	−0.8
Amoxicillin	7.0×10^{-5}	1000	4.1
Diclofenac	7.0×10^{-5}	1000	4.0
Cetirizine	7.0×10^{-5}	1000	4.1
Acetaminophen	7.0×10^{-5}	1000	3.7
Aspirin	5.2×10^{-5}	750	−3.9
Penicillin	4.9×10^{-5}	700	−8.1
Erythromycin	7.0×10^{-5}	1000	3.7
Ceftriaxime	7.0×10^{-5}	1000	4.1

Table 5
MTX determination in spiked plasma samples.

Sample	Added (M)	Found (M)	Recovery (%)
Plasma	0.0	ND	–
	5.0×10^{-9}	5.5×10^{-9}	110.0
	1.0×10^{-8}	1.0×10^{-8}	100.2
	5.0×10^{-8}	4.4×10^{-8}	88.0
	1.0×10^{-7}	1.1×10^{-7}	110.0
	5.0×10^{-7}	4.8×10^{-7}	96.3
	5.0×10^{-6}	5.7×10^{-6}	114.6

ND, not detected.

suggested the excellent potential of the ratiometric fluorescence B-GQDs/Au NSt-RB sensor for detecting MTX in actual plasma samples.

CRediT authorship contribution statement

Masoud Gazizadeh: Writing – original draft, Methodology, Investigation, Formal analysis. **Masoumeh Foroutan Koudehi:** Writing – review & editing, Supervision, Resources, Project administration. **Hossein Fasihi:** Writing – original draft, Methodology, Investigation, Formal analysis. **Jafar Soleymani:** Writing – review & editing, Conceptualization, Methodology. **Ramin Zibaseresht:** Validation, Project administration, Supervision, Writing – review & editing.

Declaration of competing interest

The authors declare that they have no known competing financial interests or personal relationships that could have appeared to influence the work reported in this paper.

Acknowledgments

This work was supported by the Biomaterials and Medicinal Chemistry Research Centre, Aja University of Medical Sciences and the Pharmaceutical Analysis Research Center of Tabriz University of Medical Sciences.

References

[1] M.O. Mohammed, H.M.M. Alkubaisi, N.Q. Haj, A new prodrug and bioactivity evaluation of methotrexate based on Chitosan, Heliyon 6 (2020) e04223.
[2] A.A. Ensafi, P. Nasr-Esfahani, B. Rezaei, Simultaneous detection of folic acid and methotrexate by an optical sensor based on molecularly imprinted polymers on dual-color CdTe quantum dots, Anal. Chim. Acta 996 (2017) 64–73.
[3] J. He, J. Wang, M. Zhang, G. Shi, Selection of a structure-switching aptamer for the specific methotrexate detection, ACS Sens. 6 (2021) 2436–2441.
[4] D. Mikhaylov, P.W. Hashim, T. Nektalova, G. Goldenberg, Systemic psoriasis therapies and comorbid disease in patients with psoriasis: a review of potential risks and benefits, J Clin Aesthet Dermatol 12 (2019) 46–54.
[5] M. Nagano, T. Toda, K. Makino, H. Miki, Y. Sugizaki, H. Tomizawa, A. Isobayashi, K. Yoshimoto, Discovery of a highly specific anti-methotrexate (MTX) DNA aptamer for antibody-independent MTX detection, Anal. Chem 94 (2022) 17255–17262.
[6] V. Maksimovic, Z. Pavlovic-Popovic, S. Vukmirovic, J. Cvejic, A. Mooranian, H. Al-Salami, M. Mikov, S. Golocorbin-Kon, Molecular mechanism of action and pharmacokinetic properties of methotrexate, Mol. Biol. Rep. 47 (2020) 4699–4708.
[7] F. Karami, S. Ranjbar, Y. Ghasemi, M. Negahdaripour, Analytical methodologies for determination of methotrexate and its metabolites in pharmaceutical, biological and environmental samples, J. Pharm. Anal 9 (2019) 373–391.
[8] S.A. Alshehri, S. Wahab, M. Khalid, M.A.A. Almoyad, Optimization of chromatographic conditions via Box–Behnken design in RP-HPLC-PDA method development for the estimation of folic acid and methotrexate in bulk and tablets, Heliyon 9 (2023) e20282.
[9] D. Wu, Y. Wang, Y. Sun, N. Ouyang, J. Qian, A simple, rapid and reliable liquid chromatography–mass spectrometry method for determination of methotrexate in human plasma and its application to therapeutic drug monitoring, BMC (Biomed. Chromatogr.) 29 (2015) 1197–1202.
[10] H.-L. Cheng, S.-S. Chiou, Y.-M. Liao, C.-Y. Lu, Y.-L. Chen, S.-M. Wu, Analysis of methotrexate and its eight metabolites in cerebrospinal fluid by solid-phase extraction and triple-stacking capillary electrophoresis, Anal. Bioanal. Chem. 398 (2010) 2183–2190.
[11] K. Hansson, H. Orrling, A. Blomgren, A. Isaksson, G. Schliamser, J. Heldrup, C. Pronk, Simultaneous determination of folate and methotrexate metabolites in serum by LC-MS/MS during high-dose methotrexate therapy, J. Chromatogr. B Biomed. Appl. 1186 (2021) 123007.
[12] X. Jiang, J. Zhang, L. Xu, W. Wang, J. Du, M. Qu, X. Han, L. Yang, B. Zhao, Ultrasensitive SERS detection of antitumor drug methotrexate based on modified Ag substrate, Spectrochim. Acta Mol. Biomol. Spectrosc. 240 (2020) 118589.
[13] L. Yang, Y. Song, L. Wang, Multi-emission metal–organic framework composites for multicomponent ratiometric fluorescence sensing: recent developments and future challenges, J. Mater. Chem. B 8 (2020) 3292–3315.
[14] M. Gazizadeh, G. Dehghan, J. Soleymani, A dual-emission ratiometric fluorescent biosensor for ultrasensitive detection of glibenclamide using S-CDs/CdS quantum dots, Spectrochim. Acta Mol. Biomol. Spectrosc. 297 (2023) 122714.
[15] F.U. Rahman, A.B. Shah, M. Muhammad, F.S. Ataya, G.E.-S. Batiha, Antioxidant, antibacterial, enzyme inhibition and fluorescence characteristics of unsymmetrical thiourea derivatives, Heliyon 10 (2024) e31563.
[16] M.I. Rumaling, F.P. Chee, A. Badea, N.H. Hasbia, S. Daimb, F. Juhima, M. Duinonga, R. Rasmidia, Methods of optical spectroscopy in detection of virus in infected samples: a review, Heliyon 8 (2022) e10472.
[17] R. Jalili, A. Khataee, M.-R. Rashidi, R. Luque, Dual-colored carbon dot encapsulated metal-organic framework for ratiometric detection of glutathione, Sens Actuators B Chem 297 (2019) 126775.
[18] X.-E. Zhao, C. Lei, Y. Gao, H. Gao, S. Zhu, X. Yang, J. You, H. Wang, A ratiometric fluorescent nanosensor for the detection of silver ions using graphene quantum dots, Sens Actuators B Chem 253 (2017) 239–246.
[19] F. Qu, H. Pei, R. Kong, S. Zhu, L. Xia, Novel turn-on fluorescent detection of alkaline phosphatase based on green synthesized carbon dots and MnO2 nanosheets, Talanta 165 (2017) 136–142.
[20] N.Q. Febrianti, M.G.R. Tunggeng, I.D. Ramadhany, R.M. Asri, Y.Y. Djabir, A.D. Permana, Validation of UV–Vis spectrophotometric and colorimetric methods to quantify methotrexate in plasma and rat skin tissue: application to in vitro release, ex vivo and in vivo studies from dissolving microarray patch loaded pH-sensitive nanoparticle, Spectrochim. Acta Mol. Biomol. Spectrosc. 315 (2024) 124258.
[21] V.A. Chhabra, R. Kaur, N. Kumar, A. Deep, C. Rajesh, K.-H. Kim, Synthesis and spectroscopic studies of functionalized graphene quantum dots with diverse fluorescence characteristics, RSC Adv. 8 (2018) 11446–11454.
[22] Q. Cui, B. Xia, S. Mitzscherling, A. Masic, L. Li, M. Bargheer, H. Möhwald, Preparation of gold nanostars and their study in selective catalytic reactions, Colloids Surf. A Physicochem. Eng. Asp. 465 (2015) 20–25.
[23] M. Gazizadeh, G. Dehghan, J. Soleymani, A ratiometric fluorescent sensor for detection of metformin based on terbium–1, 10-phenanthroline–nitrogen-doped-graphene quantum dots, RSC Adv. 12 (2022) 22255–22265.
[24] A. Hasanzadeh, F. Radmanesh, J. Kiani, M. Bayandori, Y. Fatahi, A.R. Aref, M. Karimi, Photoluminescent functionalized carbon dots for CRISPR delivery: synthesis, optimization and cellular investigation, Nanotechnology 30 (2019) 135101.
[25] A.E. Stone, S. Irgen-Gioro, R. López-Arteaga, J.T. Hupp, E.A. Weiss, Encapsulating CdSe/CdS QDs in the MOF ZIF-8 enhances their photoluminescence quantum yields in the solid state, Chem. Mater. 34 (2022) 1921–1929.
[26] J. Sarkar, S. Ray, D. Chattopadhyay, A. Laskar, K. Acharya, Mycogenesis of gold nanoparticles using a phytopathogen Alternaria alternata, Bioproc. Biosyst. Eng. 35 (2012) 637–643.
[27] N.N. Dhanasekar, G.R. Rahul, K.B. Narayanan, G. Raman, N. Sakthivel, Green chemistry approach for the synthesis of gold nanoparticles using the fungus Alternaria sp, J. Microbiol. Biotechnol. 25 (2015) 1129–1135.
[28] S. Wang, J. Yu, P. Zhao, S. Guo, S. Han, One-Step synthesis of water-soluble CdS quantum dots for silver-ion detection, ACS Omega 6 (2021) 7139–7146.
[29] P.M. Chaudhari, V.M. Bind, Topical solid lipid nanoparticles based ge l of lavender essential oil for anti-inflammatory activity, Asian J. Pharmaceut. Clin. Res. 12 (2019) 175–182.
[30] T. Teymoorian, N. Hashemi, M.H. Mousazadeh, Z. Entezarian, N, S doped carbon quantum dots inside mesoporous silica for effective adsorption of methylene blue dye, SN Appl. Sci. 3 (2021) 1–14.
[31] H. Qi, Q. Li, J. Jing, T. Jing, C. Liu, L. Qiu, R. Sami, M. Helal, K.A. Ismail, A.H. Aljahani, Construction of N-CDs and calcein-based ratiometric fluorescent sensor for rapid detection of arginine and acetaminophen, Nanomaterials 12 (2022) 976–985.
[32] M. Chen, W. Luo, Z. Zhang, F. Zhu, S. Liao, H. Yang, X. Chen, Sensitive surface enhanced Raman spectroscopy (SERS) detection of methotrexate by core-shell-satellite magnetic microspheres, Talanta 171 (2017) 152–158.
[33] J.R. Flores, G.C. Peñalvo, A.E. Mansilla, M.R. Gómez, Capillary electrophoretic determination of methotrexate, leucovorin and folic acid in human urine, J. Chromatogr. B 819 (2005) 141–147.

[34] E. Begas, C. Papandreou, A. Tsakalof, D. Daliani, G. Papatsibas, E. Asprodini, Simple and reliable HPLC method for the monitoring of methotrexate in osteosarcoma patients, J. Chromatogr. Sci. 52 (2014) 590–595.
[35] N.K. Garg, G. Sharma, B. Singh, P. Nirbhavane, O.P. Katare, Quality by design (QbD)-based development and optimization of a simple, robust RP-HPLC method for the estimation of methotrexate, J. Liq. Chromatogr. Relat. Technol. 38 (2015) 1629–1637.
[36] Z. Deng, H. Li, Q. Tian, Y. Zhou, X. Yang, Y. Yu, B. Jiang, Y. Xu, T. Zhou, Electrochemical detection of methotrexate in serum sample based on the modified acetylene black sensor, Microchem. J. 157 (2020) 105058.
[37] Z. Chen, S. Qian, X. Chen, W. Gao, Y. Lin, Protein-templated gold nanoclusters as fluorescence probes for the detection of methotrexate, Analyst 137 (2012) 4356–4361.
[38] L.-Y. Wei, K.-S. Huang, H.-H. Lin, Y.-P. Wu, K.-T. Tan, Y.Y. Lee, I.-C. Chen, Kinetic mechanism of metal enhanced fluorescence by gold nanoparticle with avidin–biotin as spacer and by gold–silver core–shell nanoparticle using fluorescence lifetime image microscopy, J. Phys. Chem. C 122 (2018) 28431–28438.
[39] S. Pawar, A. Bhattacharya, A. Nag, Metal-enhanced fluorescence study in aqueous medium by coupling gold nanoparticles and fluorophores using a bilayer vesicle platform, ACS Omega 4 (2019) 5983–5990.
[40] M.T. Yaraki, Y.N. Tan, Metal nanoparticles-enhanced biosensors: synthesis, design and applications in fluorescence enhancement and surface-enhanced Raman scattering, Chem. Asian J. 15 (2020) 3180–3208.
[41] Z. Golsanamlou, H. Kholafazad-Kordasht, J. Soleymani, A. Jouyban, Quantification of methotrexate in plasma samples using highly fluorescent nanoparticles, J. Pharm. Biomed. Anal. 214 (2022) 114716.
[42] R. Shokri, M. Amjadi, A ratiometric fluorescence sensor for triticonazole based on the encapsulated boron-doped and phosphorous-doped carbon dots in the metal organic framework, Spectrochim. Acta Mol. Biomol. Spectrosc. 246 (2021) 118951.
[43] J. Soleymani, M. Hasanzadeh, N. Shadjou, M.H. Somi, A. Jouyban, Spectrofluorimetric cytosensing of colorectal cancer cells using terbium-doped dendritic fibrous nano-silica functionalized by folic acid: a novel optical cytosensor for cancer detection, J. Pharm. Biomed. Anal. 180 (2020) 113077.
[44] G. Dehghan, M. Shaghaghi, P. Alizadeh, A novel ultrasensitive and non-enzymatic "turn-on-off" fluorescence nanosensor for direct determination of glucose in the serum: as an alternative approach to the other optical and electrochemical methods, Spectrochim. Acta Mol. Biomol. Spectrosc. 214 (2019) 459–468.